Tb3+ doped Ga5Ge20Sb10Se65-xTex (x=0-37.5) chalcogenide glasses and fibers for MWIR and LWIR emissions

N. Abdellaoui, F. Starecki, Catherine Boussard-Plédel, Y. Shpotyuk, J-L. Doualan, A. Braud, E. Baudet, P. Nemec, François Cheviré, Marc Dussauze, et al.

Research Article | Vol. 8, No. 9 | 1 Sep 2018 | OPTICAL MATERIALS EXPRESS 2887
Optical Materials EXPRESS

Tb^{3+} doped $Ga_5Ge_{20}Sb_{10}Se_{65-x}Te_x$ (x = 0-37.5) chalcogenide glasses and fibers for MWIR and LWIR emissions

N. Abdellaoui,[1] F. Starecki,[2] C. Boussard-Pledel,[1] Y. Shpotyuk,[1] J-L. Doualan,[2] A. Braud,[2] E. Baudet,[3] P. Nemec,[3] F. Cheviré,[1] M. Dussauze,[4] B. Bureau,[1] P. Camy,[2] and V. Nazabal[1,*]

[1]*Laboratoire Verres et Céramiques UMR-CNRS 6226, Université de Rennes, 35042 Rennes, France*
[2]*Centre de Recherche sur les Ions, les Matériaux et la Photonique (CIMAP), UMR 6252 CEA-CNRS-Ensicaen, Université de Caen, 6 Boulevard du Maréchal Juin, 14050 Caen cedex 4, France*
[3]*Department of Graphic Arts and Photophysics, Faculty of Chemical Technology, University of Pardubice, 53210 Pardubice, Czech Republic*
[4]*Institut des Sciences Moléculaires, Université de Bordeaux, 33405 Talence, France*
**virginie.nazabal@univ-rennes1.fr*

Abstract: Chalcogenide glasses with a nominal composition of $Ga_5Ge_{20}Sb_{10}Se_{(65-x)}Te_x$ (x = 0, 10, 20, 25, 30, 32.5, 35, 37.5) were synthesized. Their physico-chemical properties, glass network structure and optical properties are clearly modified via the substitution of selenium by tellurium. Based on a detailed study of the $Ga_5Ge_{20}Sb_{10}Se_{(65-x)}Te_x$ bulk glasses properties, the $Ga_5Ge_{20}Sb_{10}Se_{45}Te_{20}$ seleno-telluride glass optimal composition has been selected for fiber drawing. The luminescence properties of Tb^{3+}(500 ppm) doped $Ga_5Ge_{20}Sb_{10}Se_{65}$ and $Ga_5Ge_{20}Sb_{10}Se_{45}Te_{20}$ bulk glasses and fibers were studied. Radiative transitions parameters calculated from the Judd-Ofelt theory are compared to the experimental values. Mid-wavelength infrared emission in the range of 4.3-6.0 µm is attributed to the $^7F_5 \rightarrow {}^7F_6$ transition of Tb^{3+}ions with a corresponding experimental lifetime of 8.9 and 7.8 ms for the selenide and seleno-telluride matrix, respectively. The $^7F_4 \rightarrow {}^7F_6$ emission was recorded at 3.1 µm with a good signal-to-noise ratio, evidencing a rather strong emission from the $^7F_4$ manifold. Finally, although it was expected that the phonon energy will be lower for telluride glasses, selenide glasses are still more suitable for mid-wavelength infrared and long wavelength infrared emissions with well-defined emissions from 3.1 to 8 µm.

OCIS codes: (160.2750) Glass and other amorphous materials; (160.5690) Rare-earth-doped materials; (160.2290) Fiber materials.

References and links

1. S. Cui, R. Chahal, C. Boussard-Plédel, V. Nazabal, J. L. Doualan, J. Troles, J. Lucas, and B. Bureau, "From selenium- to tellurium-based glass optical fibers for infrared spectroscopies," Molecules **18**(5), 5373–5388 (2013).
2. F. Starecki, F. Charpentier, J.-L. Doualan, L. Quetel, K. Michel, R. Chahal, J. Troles, B. Bureau, A. Braud, P. Camy, V. Moizan, and V. Nazabal, "Mid-IR optical sensor for CO_2 detection based on fluorescence absorbance of Dy^{3+}:$Ga_5Ge_{20}Sb_{10}S_{65}$ fibers," Sens. Actuators B Chem. **207**, 518–525 (2015).
3. S. Danto, P. Houizot, C. Boussard-Pledel, X. Zhang, F. Smektala, and J. Lucas, "A Family of Far-Infrared-Transmitting Glasses in the Ga–Ge–Te System for Space Applications," Adv. Funct. Mater. **16**(14), 1847–1852 (2006).
4. S. Cui, C. Boussard-Plédel, J. Troles, and B. Bureau, "Telluride glass single mode fiber for mid and far infrared filtering," Opt. Mater. Express **6**(4), 971–978 (2016).
5. B. Bureau, C. Boussard-Pledel, P. Lucas, X. Zhang, and J. Lucas, "Forming glasses from Se and Te," Molecules **14**(11), 4337–4350 (2009).
6. V. Shiryaev, M. Churbanov, J.-L. Adam, and X. Zhang, "Chalcogenide waveguide for infrared sensing" in *Chalcogenide Glasses* (Woodhead Publishing, 2014).
7. L. B. Shaw, D. Schaafsma, J. Moon, B. Harbison, J. S. Sanghera, and I. D. Aggawal, "Evaluation of the IR transitions in rare-earth-doped chalcogenide glass," in Proc. Conf. Lasers and Electro-Optics (OSA), Washington, DC, 1997, p. 255.

#334152 https://doi.org/10.1364/OME.8.002887
Journal © 2018 Received 1 Jun 2018; revised 15 Aug 2018; accepted 15 Aug 2018; published 29 Aug 2018

Optical Materials EXPRESS

8. Ya. Shpotyuk, A. Ingram, O. Shpotyuk, C. Boussard-Pledel, V. Nazabal, and B. Bureau, "Effect of rare-earth doping on the free-volume structure of Ga-modified $Te_{20}As_{30}Se_{50}$ glass," RSC Advances **6**(27), 22797–22802 (2016).
9. Ł. Sójka, Z. Tang, H. Zhu, E. Bereś-Pawlik, D. Furniss, A. Seddon, T. Benson, and S. Sujecki, "Study of mid-infrared laser action in chalcogenide rare earth doped glass with Dy^{3+}, Pr^{3+} and Tb^{3+}," Opt. Mater. Express **2**(11), 1632–1640 (2012).
10. M. E. Webber, M. Pushkarsky, and C. K. N. Patel, "Optical detection of chemical warfare agents and toxic industrial chemicals: Simulation," J. Appl. Phys. **97**(11), 113101 (2005).
11. L. B. Shaw, B. Cole, P. A. Thielen, J. S. Sanghera, and I. D. Aggarwal, "Mid-wave IR and long-wave IR laser potential of rare-earth doped chalcogenide glass fiber," IEEE J. Quantum Electron. **37**(9), 1127–1137 (2001).
12. F. Starecki, N. Abdellaoui, A. Braud, J.-L. Doualan, C. Boussard-Plédel, B. Bureau, P. Camy, and V. Nazabal, "8 μm luminescence from a Tb^{3+} GaGeSbSe fiber," Opt. Lett. **43**(6), 1211–1214 (2018).
13. M. F. Churbanov, I. V. Scripachev, V. S. Shiryaev, V. G. Plotnichenko, S. V. Smetanin, E. B. Kryukova, Yu. N. Pyrkov, and B. I. Galagan, "Chalcogenide glasses doped with Tb, Dy and Pr ions," J. Non-Cryst. Solids **326–327**(1), 301–305 (2003).
14. L. Sojka, Z. Tang, D. Furniss, H. Sakr, Y. Fang, E. Beres-Pawlik, T. Benson, A. Seddon, and S. Sujecki, "Mid-infrared emission in Tb^{3+} doped selenide glass fiber," J. Opt. Soc. Am. B **34**(3), A70–A79 (2017).
15. V. Shiryaev, M. Churbanov, J.-L. Adam, and X. Zhang, "Preparation of high-purity chalcogenide glasses" in *Chalcogenide Glasses* (Woodhead Publishing, 2014).
16. R. Hui and M. O'Sullivan, *Fiber Optic Measurement Techniques* (Academic, 2009), Chap. 4.
17. I. Pethes, R. Chahal, V. Nazabal, C. Prestipino, S. Michalik, J. Darpentigny, and P. Jóvári, "Chemical order in Ge-Ga-Sb-Se glasses," J. Non-Cryst. Solids **484**, 49–56 (2018).
18. S. Sugai, "Stochastic random network model in Ge and Si chalcogenide glasses," Phys. Rev. B Condens. Matter **35**(3), 1345–1361 (1987).
19. G. Lucovsky, C. K. Wong, and W. B. Pollard, "Vibrational properties of glasses: Intermediate range order," J. Non-Cryst. Solids **59–60**(Part 2), 839–846 (1983).
20. P. Nemec, B. Frumarová, and M. Frumar, "Structure and properties of the pure and Pr^{3+}-doped $Ge_{25}Ga_5Se_{70}$ and $Ge_{30}Ga_5Se_{65}$ glasses," J. Non-Cryst. Solids **270**(1-3), 137–146 (2000).
21. K. Jackson, A. Briley, S. Grossman, D. V. Porezag, and M. R. Pederson, "Raman-active modes of α – $GeSe_2$ and α – GeS_2 : A first-principles study, " Phys. Rev. B **60**(22), R14985 (1999).
22. C. Gonçalves, "Telluride glasses for infrared optics: a structural approach by vibrationnal spectroscopies and NMR," (Rennes University, 2017).
23. R. Holomb, V. Mitsa, E. Akalin, S. Akyuz, and M. Sichka, "Ab initio and Raman study of medium range ordering in GeSe2 glass," J. Non-Cryst. Solids **373-374**, 51–56 (2013).
24. D. R. Goyal and A. S. Maan, "Far-infrared absorption in amorphous $Sb_{15}Ge_xSe_{85-x}$ glasses," J. Non-Cryst. Solids **183**(1-2), 182–185 (1995).
25. M. D. Rechtin, A. R. Hilton, and D. J. Hayes, "Infrared transmission in GE-SB-SE glasses," J. Electron. Mater. **4**(2), 347–362 (1975).
26. G. Lucovsky, A. Mooradian, W. Taylor, G. B. Wright, and R. C. Keezer, "Identification of fundamental vibrational modes of trigonal alpha-monoclinic and amorphous selenium," Solid State Commun. **5**(2), 113–117 (1967).
27. V. Nazabal, P. Nemec, A. M. Jurdyc, S. Zhang, F. Charpentier, H. Lhermite, J. Charrier, J. P. Guin, A. Moreac, M. Frumar, and J. L. Adam, "Optical waveguide based on amorphous Er^{3+}-doped Ga-Ge-Sb-S(Se) pulsed laser deposited thin films," Thin Solid Films **518**(17), 4941–4947 (2010).
28. I. Voleska, J. Akola, P. Jovari, J. Gutwirth, T. Wagner, T. Vasileiadis, S. N. Yannopoulos, and R. O. Jones, "Structure, electronic, and vibrational properties of glassy $Ga_{11}Ge_{11}Te_{78}$: Experimentally constrained density functional study," Phys. Rev. B **86**(9), 094108 (2012).
29. P. Nemec, V. Nazabal, M. Dussauze, H. L. Ma, Y. Bouyrie, and X. H. Zhang, "Ga-Ge-Te amorphous thin films fabricated by pulsed laser deposition," Thin Solid Films **531**, 454–459 (2013).
30. S. Sen, E. L. Gjersing, and B. G. Aitken, "Physical properties of $Ge_xAs2_xTe100_{-3x}$ glasses and Raman spectroscopic analysis of their short-range structure," J. Non-Cryst. Solids **356**(41-42), 2083–2088 (2010).
31. A. Mendoza-Galvan, E. Garcia-Garcia, Y. V. Vorobiev, and J. Gonzalez-Hernandez, "Structural, optical and electrical characterization of amorphous SeTe thin film alloys," Microelectron. Eng. **51–52**, 677–687 (2000).
32. P. Nemec, V. Nazabal, A. Moreac, J. Gutwirth, L. Benes, and M. Frumar, "Amorphous and crystallized Ge-Sb-Te thin films deposited by pulsed laser: Local structure using Raman scattering spectroscopy," Mater. Chem. Phys. **136**(2-3), 935–941 (2012).
33. K. S. Andrikopoulos, S. N. Yannopoulos, A. V. Kolobov, P. Fons, and J. Tominaga, *Raman Scattering Study of GeTe and $Ge_2Sb_2Te_5$ Phase-change Materials* (Elsevier, 2007).
34. G. C. Sosso, S. Caravati, R. Mazzarello, and M. Bernasconi, "Raman spectra of cubic and amorphous $Ge_2Sb_2Te_5$ from first principles," Phys. Rev. B **83**(13), 134201 (2011).
35. F. Charpentier, F. Starecki, J. Doualan, P. Jóvári, P. Camy, J. Troles, S. Belin, B. Bureau, and V. Nazabal, "Mid-IR luminescence of Dy^{3+} and Pr^{3+} doped $Ga_5Ge_{20}Sb_{10}S(Se)_{65}$ bulk glasses and fibers," Mater. Lett. **101**, 21–24 (2013).
36. Z. Yang, O. Gulbiten, P. Lucas, T. Luo, and S. Jiang, "Long-wave infrared-transmitting optical fibers," J. Amer. Cer. Soc. **94**(6), 1761–1765 (2011).

Optical Materials EXPRESS

37. W. T. Carnall, P. R. Fields, and B. G. Wybourne, "Spectral Intensities of the Trivalent Lanthanides and Actinides in Solution. I. Pr^{3+}, Nd^{3+}, Er^{3+}, Tm^{3+}, and Yb^{3+}," J. Chem. Phys. **42**(11), 37973 (1965).

1. Introduction

Due to their wide infrared transparency and the possibility of incorporation of rare earth ions active in mid-wavelength infrared spectral range, chalcogenide glasses are good candidates to build all optical gas sensors. To detect and quantify gases, one way is to develop chalcogenide glasses presenting transparency compatible with the absorption band frequency of these molecules. Here, two domains of interest can be distinguished: mid-wavelength infrared (MWIR) and long wavelength infrared (LWIR) corresponding to the 3–5 and 8–12 μm spectral ranges, respectively. The expanded wavelength range will enable a variety of commercial and military applications, such as allowing sensors to be tuned to detect atmospheric trace gases for air quality evaluation or hazard alerts. Selenide-and sulfide-based chalcogenide glasses are known for their excellent infrared transmission within the 1-15 μm region with satisfactory thermo-mechanical properties [1]. Doped with Dy^{3+}, sulfide glass fibers have been used as MWIR source for gas sensor applied to CO_2 detection [2]. To probe the infrared region beyond 12 μm, telluride glasses appear as an attractive material due to its low phonon energy and broad transparency window (up to 25 μm) [1,3,4]. Despite their interesting optical properties, especially for LWIR, there are only few studies focused on the incorporation of rare earths into telluride glasses. This can be explained by the difficulties to obtain a vitreous network because the Te-based glasses have strong tendency to crystallize which may penalize the incorporation of rare earths and their luminescence properties [5]. To overcome the tendency to crystallization of telluride glasses, one possible way is to add selenium. Indeed, for each glassy system, it is required to determine the best compromise between suitable transparency domain for optical excitation, low phonon energy and glass state stability by optimizing the ratio between selenium and tellurium content. For example, it has been previously shown that with appropriate ratio between Se and Te in As-Se-Te glasses, it is possible to draw fiber with optical attenuation below 1dB/m and a transparency domain between 1.5 and 18 μm [6]. The doping of telluride glass with Tb^{3+} ions [7] and Ga-modified $As_{30}Se_{50}Te_{20}$ glass with Pr^{3+} ions [8] has been reported; however, it only concerned the emissions in MWIR. Following the energy level diagram of Tb^{3+} ion, one can expect to have several radiative emissions from 3.1 up to 8 μm. Theoretical work demonstrated that Tb^{3+} doped chalcogenide glass is an excellent candidate for laser application at 7.5 μm [9]. For gas sensor applications, this is a wavelength range of interest due to the LWIR absorption band of some hazardous gases [10]. To the best of our knowledge, only two papers report the measurement of the photoluminescence originating from the $^7F_4 \rightarrow {}^7F_5$ transition of Tb^{3+}ions. The first observation of this radiative emission was confirmed at 7.5 μm for Ge-As-Ga-Se glass doped with 1000 ppm of Tb^{3+} [11]. More recently, Starecki *et al.* published a comprehensive study of the 8 μm fluorescence of Tb^{3+}ions incorporated in Ga-Ge-Sb-Se fiber [12]. It is worthy to mention the work of Churbanov *et al.,* who investigated Tb^{3+} luminescence (4-5 μm region) in chalcogenide glasses based on As-Se and As-S-Se [13]. They fabricated Tb^{3+} doped optical fibers with 1.5 dB/m optical loses at 6-9 μm which implies a low level of impurities. However the Tb^{3+} emissions from the $^7F_4$ level at 3.1 μm ($^7F_4 \rightarrow {}^7F_6$) and at 7.5 μm ($^7F_4 \rightarrow {}^7F_5$) were not observed. The highest lifetime of 16.3 ms for the $^7F_5$ level was reached with the glass presenting the minimum content of Se-H and S-H entities (43 ppm and 4 ppm respectively). Contrary, for the glass containing the highest impurities concentration (226 ppm for Se-H and 235 ppm for S-H) the lifetime falls to 1.5 ms. Lately, Sojka *et al* studied the MWIR emission behavior of Tb^{3+} doped As-Ga-Ge-Se bulk glasses and conventional fibers. A broad emission band corresponding to the $^7F_5 \rightarrow {}^7F_6$ transition was observed at 4.7 μm with a measured lifetime of 12.9 ms ($\tau_{rad\text{-}JO}$ = 13.1 ms) [14].

In this study we characterize the vitreous network of $Ga_5Ge_{20}Sb_{10}Se_{(65-x)}Te_x$ (x = 0, 10, 20, 25, 30, 32.5, 35, 37.5) system and investigate the physico-chemical properties of these

Optical Materials EXPRESS

glasses. First, the influence of substitution of tellurium instead of selenium on the glass properties is evaluated (IR transmission properties, phonon energy, refractive index, density, T_g and T_x). Second, we discuss the photoluminescence properties of Tb^{3+} (500 ppm) doped $Ga_5Ge_{20}Sb_{10}Se_{65}$ and $Ga_5Ge_{20}Sb_{10}Se_{45}Te_{20}$ bulk glasses and optical fibers. The experimental luminescence data are compared to radiative parameters calculated via Judd-Ofelt (J-O) theory.

2. Experimental procedure

2.1 Glass synthesis and basic characterizations

Tb^{3+} doped chalcogenide glasses studied in this paper belong to the Ga-Ge-Sb-Se-Te system. The fabricated compositions are $Ga_5Ge_{20}Sb_{10}Se_{65-x}Te_x$ with x ranging from 0 to 37.5% undoped or doped with Tb^{3+} (500 ppm) for x = 0 and 20. These glasses were prepared by means of conventional melting and quenching method. High purity raw materials were used for glass preparation, *e.g.* Ge (5N, Umicore), Ga (7N, Alpha), Sb (5N, Alpha), Tb_2Se_3 (3N, non-commercial); Se (5N, Umicore) and Te (5N, JGI) were further purified by successive distillations (dynamic as well as static distillation) to remove carbon and hydrates impurities. Then, the required amounts of chemical reagents were introduced into silica ampoules inside the gloved box and pumped under vacuum for a few hours. After the pumping, the silica tubes were sealed and heated up to850°C during a total heating process time of 17 hours in a rocking furnace to ensure the homogenization of the melt. After water quenching, the glass rods were annealed near their glass transition temperatures for 3h. The preform of 7 mm in diameter and approximately 10 cm length was drawn in single refractive index fibers with 350 µm diameter.

For the physico-chemical characterizations of bulk glass samples, the remainders of the initial preform after fiber drawing were cut and polished to 5 mm thick disks. Characteristic temperatures (glass transition temperature T_g and crystallization temperature T_x) for each glass sample were determined with an accuracy of ± 2 °C using a differential scanning calorimeter DSC 2010 (TA Instruments), with a heating rate of 10 °C/min between room temperature and 380°C. The density of the glasses was measured using Archimedes' principle. The composition of the different samples was checked by using scanning electron microscopy with an energy-dispersive X-ray analyzer (SEM-EDS, JSM 6400 – Oxford Link INCA). The Se-H content in the glasses was determined by IR-spectroscopy exploiting the measured absorption coefficient and known value of the extinction coefficient at 4.5 µm (ε = 1000 dB/km/ppm) [15].

2.2 Optical measurements

The ground state absorption measurements were performed with a double-beam Perkin–Elmer spectrophotometer in the wavelength range of 800–3200 nm and a resolution of 1 nm. For bulk glasses, transmission spectra in the IR region were recorded with a Bruker Vector 22 Fourier transformed infrared spectrometer (FTIR) from 1.5 to 22 µm. Fiber attenuation measurements were performed for unclad Tb^{3+}doped $Ga_5Ge_{20}Sb_{10}Se_{65-x}Te_x$ (x = 0, 20) fibers and undoped $Ga_5Ge_{20}Sb_{10}Se_{65-x}Te_x$ (x = 0, 20) by using the cut-back technique [16] with a Bruker FTIR spectrometer modified with fiber coupling ports.

For room-temperature photoluminescence measurements, the pump laser light was either focused into a bulk glass sample with a silica lens or coupled into the terbium doped $Ga_5Ge_{20}Sb_{10}Se_{(65-x)}Te_x$ (x = 0, 20) fiber. The pump source at 2.05 µm for bulk and fiber experiments was a homemade laser with a Tm^{3+}:YAG crystal pumped by a commercial diode at 785 nm. The mid-IR light focused on the monochromator slit was detected by a nitrogen cooled HgCdTe detector. Fluorescence decays were measured using 30 ms pump pulses with a 9 Hz repetition rate. Emission spectra were measured with appropriate long-pass filters and corrected using an Arcoptix MWIR-2.0-9.0 blackbody source.

Optical Materials EXPRESS

The structure of $Ga_5Ge_{20}Sb_{10}Se_{65-x}Te_x$ (x ranging from 0 to 37.5%) glasses was investigated using a LabRamHR800 (Horiba-Jovin-Yvon) confocal micro-Raman spectrophotometer with 785 nm laser diode coupled to Olympus × 100 microscope. To avoid photoinduced phenomena, optical density filters have been selected to reduce the laser power focused on the glass samples. Infrared measurements were also performed with a FTIR vacuum spectrometer (Bruker Vertex 70V, equipped with Hg arc source) to cover the frequency range from 30 to 1000 cm^{-1}. The infrared spectra of bulk glasses were recorded in the reflectance mode at quasi normal incidence (11°), and the complex refractive index of each sample was obtained through Kramers-Krönig analysis of its specular reflectance spectrum. The infrared spectra reported in this work are in the form of absorption coefficient spectra, α(ν), calculated from the relation $\alpha(\nu) = 4\pi\nu k(\nu) = 2\pi\nu\varepsilon''(\nu)/n(\nu)$, where $n(\nu)$ and $k(\nu)$ are the real and imaginary parts, respectively, of the complex refractive index, $\varepsilon''(\nu)$ is the imaginary part of the dielectric function and ν is the infrared frequency (in cm^{-1}).

Linear refractive indices were obtained from the analysis of variable angle spectroscopic ellipsometry (VASE) data measured in NWIR-LWIR spectral range (1-12 μm) (J. A. Woollam Co., Inc., Lincoln, NE, USA). The VASE measurements parameters are as follows: angles of incidence of 65°, 70° and 75°. To derive refractive indices in NWIR–LWIR spectral range, Sellmeier dispersion relation was exploited, setting extinction coefficient in first approximation to zero. X-ray diffraction (XRD) patterns were recorded at room temperature in the 2θ range 15°-120° with a step size of 0.026° and a scan time per step of 400 s using a PANalytical X'Pert Pro diffractometer (PANalytical, Almelo, The Netherlands, Cu K-L2,3 radiation, λ = 1.5418 Å, PIXcel 1D detector). Data Collector and HighScore Plus software packages were used, respectively, for recording and analyzing the patterns.

3. Results and discussion

3.1. Glass composition and optical properties

Table 1. Chemical composition of $Ga_5Ge_{20}Sb_{10}Se_{(65-x)}Te_x$ (x = 0 - 37.5) undoped samples and $Ga_5Ge_{20}Sb_{10}Se_{(65-x)}Te_x$ (x = 0, 20) doped with Tb^{3+} (500 ppm), Se-H concentration (ppm) and glass stability criterion ΔT(°C).

Sample	Theoretical composition	EDS experimental composition (± 1%)	[Se-H] (ppm) (± 1 ppm)	ΔT (°C) (± 2 °C)
x = 0	$Ga_5Ge_{20}Sb_{10}Se_{65}$	$Ga_5Ge_{20}Sb_{10}Se_{65}$	33	> 150
x = 10	$Ga_5Ge_{20}Sb_{10}Se_{55}Te_{10}$	$Ga_5Ge_{20}Sb_{10}Se_{55}Te_{10}$	23	> 150
x = 20	$Ga_5Ge_{20}Sb_{10}Se_{45}Te_{20}$	$Ga_5Ge_{20}Sb_{10}Se_{45}Te_{19}$	20	> 150
x = 25	$Ga_5Ge_{20}Sb_{10}Se_{40}Te_{25}$	$Ga_5Ge_{20}Sb_{10}Se_{40}Te_{24}$	33	134
x = 30	$Ga_5Ge_{20}Sb_{10}Se_{35}Te_{30}$	$Ga_6Ge_{19}Sb_{11}Se_{35}Te_{30}$	16	120
x = 32.5	$Ga_5Ge_{20}Sb_{10}Se_{32.5}Te_{32.5}$	$Ga_5Ge_{20}Sb_{11}Se_{32}Te_{32}$	13	100
x = 35	$Ga_5Ge_{20}Sb_{10}Se_{30}Te_{35}$	$Ga_5Ge_{20}Sb_{11}Se_{30}Te_{34}$	8	84
x = 37.5	$Ga_5Ge_{20}Sb_{10}Se_{27.5}Te_{37.5}$	$Ga_6Ge_{19}Sb_{10}Se_{28}Te_{37}$	4	73 glass-ceramics
x = 0: Tb^{3+}	$Ga_5Ge_{20}Sb_{10}Se_{65}$	$Ga_5Ge_{20}Sb_{10}Se_{65}$	-	> 150
x = 20:Tb^{3+}	$Ga_5Ge_{20}Sb_{10}Se_{45}Te_{20}$	$Ga_5Ge_{20}Sb_{10}Se_{45}Te_{19}$	-	> 150

Table 1 summarizes the samples synthesized in the Ga-Ge-Sb-Se-Te system with composition of $Ga_5Ge_{20}Sb_{10}Se_{65-x}Te_x$ (x = 0, 10, 20, 25, 30, 32.5, 35, 37.5) undoped and doped with 500 ppm of Tb^{3+} for $Ga_5Ge_{20}Sb_{10}Se_{65}$ and $Ga_5Ge_{20}Sb_{10}Se_{45}Te_{20}$ glasses. Theoretical chemical composition, EDS experimental composition, [Se-H] concentration and $\Delta T(T_x-T_g)$ are

Optical Materials EXPRESS

reported. The substitution of tellurium instead of selenium shows that glassy matrices were obtained up to 35 at.% of Te as confirmed by X-ray diffraction data.

For the composition with the highest tellurium content (x = 37.5%), a glass-ceramic was obtained due to negative influence of tellurium decreasing the glass-forming ability. XRD pattern displayed in Fig. 1(a) shows that the glass-ceramic sample contains large amount of an amorphous phase with some crystallites of $GeSb_2Te_4$ (JCPDS: 01-075-1024), Ga_2Te_3 (JCPDS: 00-035-1490) and Te (JCPDS: 01-085-0557) phases.

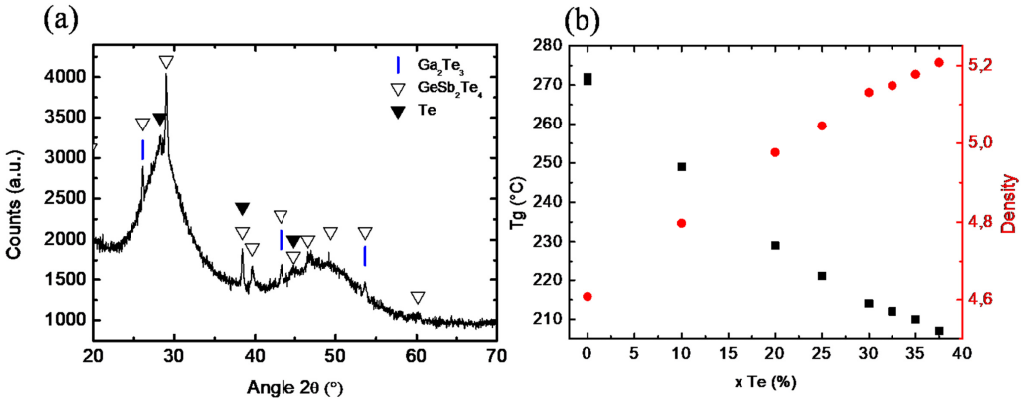

Fig. 1. (a) X-ray diffraction pattern of $Ga_5Ge_{20}Sb_{10}Se_{27.5}Te_{37.5}$ glass-ceramic sample with crystallites of Ga_2Te_3, $GeSb_2Te_4$ and Te, (b) density (± 0.01) and Tg (± 5°C) versus Te content in$Ga_5Ge_{20}Sb_{10}Se_{65-x}Te_x$ glasses.

For all the glass samples, the experimental composition data are in good agreement with the nominal ones. The increase of the Te concentration leads to a linear increase in the density ($Z_{Te}>Z_{Se}$ with Z the atomic number) and to the reduction of the glass transition temperature T_g from 272 °C to 210 °C (Fig. 1(b)). This trend is also accompanied by the decrease of glass stability criterion ΔT with increasing content of Te in studied glasses (Table 1). In detail, ΔT falls below 100 °C for content of Te >32.5 at. %, which makes those compositions less suitable for fiber applications [4]. It is interesting to note that for a relatively subtle increase of Te concentration, from 30 to 32.5 at.%, T_g is stable (215 and 212 °C, respectively), but ΔT decrease significantly (20°C) which confirms a strong influence of Te on glass-forming ability/glass stability.

Figures 2(a) and (b)show the absorption coefficient of $Ga_5Ge_{20}Sb_{10}Se_{65-x}Te_x$ glasses in the near and mid-IR respectively. The cut-off wavelengths (inset of Fig. 2(a).) are red-shifted with the introduction of Te atoms which are heavier than the Se ones. Heavier Te atoms change average bond energies of the glass network leading to the shift of multiphonon absorption edge in mid-IR (Fig. 2(b).) and modification of the electronic structure resulting in red-shift of electronic band-gap in the near-IR (Fig. 2(a).). Based on FTIR measurements, [Se-H] concentration, reported in Table 1, varies from 33 to 8 ppm with increasing Te content from x = 0 to x = 35. At the same time, the content of hydroxyl group [O-H] (absorption peak around 2.8-3.3 µm) increases by adding tellurium. This result means that seleno-telluride glasses could present non-radiative relaxation involving [O-H] entities with higher phonon energy than [Se-H] mostly observed in pure selenide glass. Note that the concentration of [Te-H] which absorbs around 5.1 µm [4] does not increase significantly with increasing Te content.

Optical Materials EXPRESS

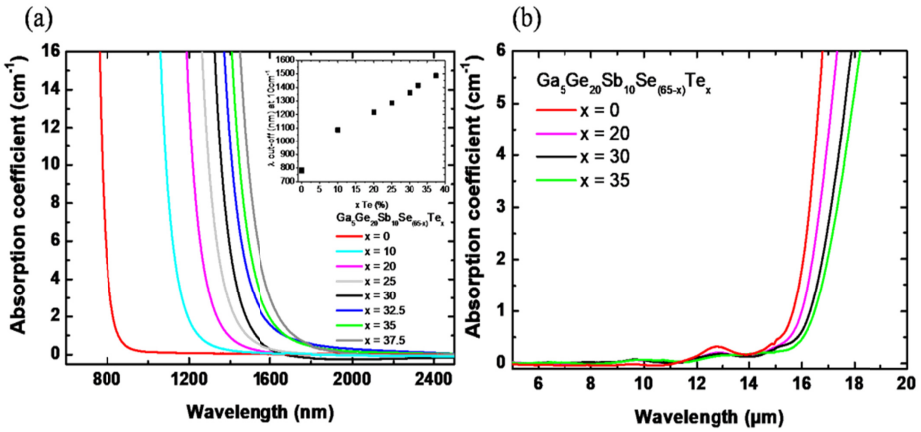

Fig. 2. (a) Absorption coefficient α for the 700-2500 nm wavelength domain; inset shows the cut-off wavelength defined at α = 10 cm^{-1} (b) absorption coefficient in 5-20 μm spectral range.

The local structure of the $Ga_5Ge_{20}Sb_{10}Se_{65-x}Te_x$ glasses was determined by far-IR and Raman spectroscopy (Fig. 3). The observation of the vibrational bands measured by Raman and infrared spectroscopy is governed by dissimilar selection rules. The almost complete overview of the spectral signatures of the material can be achieved by coupling these two techniques relating the characteristic phonon frequencies to the vibrations of local structure entities forming the glass structure. It is expected that almost all the fundamental vibrational modes can appear in both, infrared absorption and Raman spectra because of partial breakdown of selection rules in glassy materials; however, clear difference in magnitude of individual vibrational modes will be observed and some of them might be still completely extinct. The precise knowledge of the phonon frequency distribution of the glass network makes possible to assess better its implication in the non-radiative relaxation processes of the rare earth ions in the glass matrix.

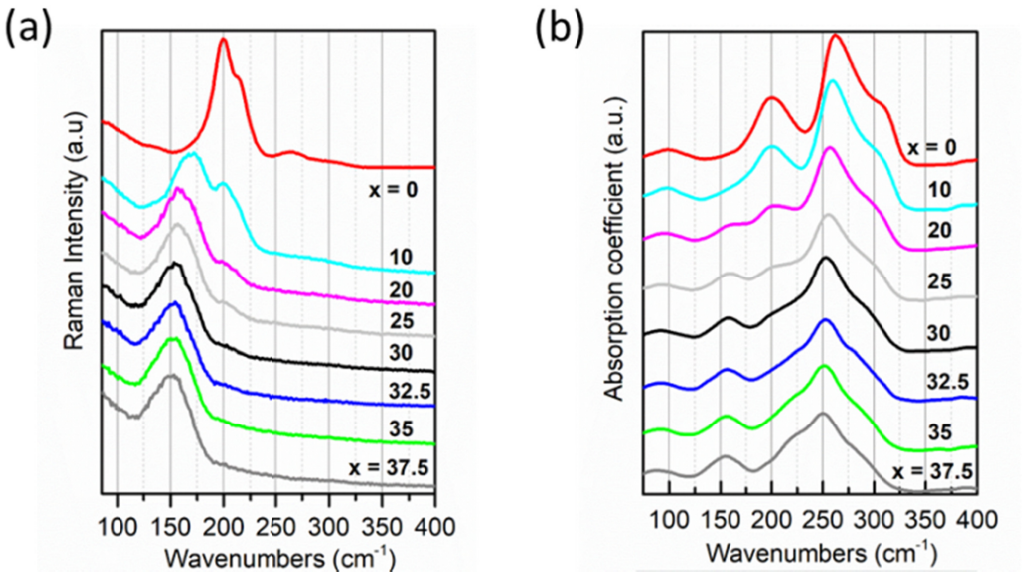

Fig. 3. (a) Far-infrared absorption spectra and (b) Raman scattering spectra of bulk $Ga_5Ge_{20}Sb_{10}Se_{65-x}Te_x$glasses.

Optical Materials EXPRESS

The structure of $Ga_5Ge_{20}Sb_{10}Se_{65}$glasscan be described by the chemically ordered network model: the Ge–Se, Ga–Se and Sb–Se bonds are the most prominent while Ge–Ge and Ge–Sb bonds were proposed to be formed especially in Se-poor compositions [17].Considering the [$GeSe_{4/2}$] entities, the IR bands peaking at ~262 and 305 cm^{-1} are assigned to their antisymmetric stretching modes while the main Raman bands located at 200 and 215 cm^{-1} have been attributed, respectively, to the localized modes of A_1symmetric stretching vibration mode of corner-sharing [$GeSe_{4/2}$] tetrahedra (Td-CS) and A_{c1} often called "companion" mode, corresponding to the vibration in edge-sharing tetrahedral (Td-ES) [18–20]. This attribution was also confirmed by calculation of vibrational normal modes of cluster models by means of first-principles method based on the density-functional theory (DFT) [21–23]. Given the closeness of gallium and germanium in terms of atomic weights (Ga: 69.72, Ge: 72.59) and structural units ([Ge(Ga)$Se_{4/2}$] tetrahedra) involved in selenide glass matrix, it is quite challenging to discern [$GeSe_{4/2}$] and [$GaSe_{4/2}$] specific vibrational modes since the concentration of gallium is limited to only 5 at.%. The presence of antimony in $Ga_5Ge_{20}Sb_{10}Se_{65}$ glass has also a widening effect on the main band compared to the Ge-Se binary glass system. At lower energy side, the [$SbSe_{3/2}$] pyramids have a symmetric stretching vibration mode at 190 cm^{-1}. This assignment was also proposed for an IR spectra contribution at 180 cm^{-1}in Ge-Sb-Se system [24, 25]; similarly, the IR band at 200 cm^{-1} can be attributed to [$SbSe_{3/2}$] entities vibrations. In Raman spectra, the 235-270 cm^{-1} spectral range includes the stretching vibration of Se-Se bonds with a wide distribution of vibration modes depending on the nature or length of Se–Se chains. The vibration modes were attributed to (i) Se-Se at the outrigger-raft cluster and/or long Se_n-Se chain vibrations (~235 cm^{-1}), (ii) A_1 stretching mode of Se_8 ring molecules (245-250 cm^{-1}) and (iii) Se_n-Se small short chains of [Ge(Ga)$Se_{4/2}$] or [$SbSe_{3/2}$] structural units where at least one of the selenium at the tetrahedron or pyramid corner is linked to another selenium(~265 cm^{-1}) [20]. The specific stoichiometry of the $Ga_5Ge_{20}Sb_{10}Se_{65}$ glass results in a relatively low proportion of Se-Se bonds which are involved in short chains as evidenced by the moderate amplitude of the broad band at 265 cm^{-1}.Polymeric chains of Se can also be observed with a minor band at 135 cm^{-1} for IR and 138 cm^{-1} for Raman active modes, according to Lucovsky [26]. The presence of homopolar bonds in this stoichiometric glass is related to atomic disorder and some "wrong" Ge-Ge and Se-Se bonds can still be found in low concentrations. At low-energy side (150-175cm^{-1}), the vibration modes are usually connected with the stretching vibration modes of the M-M bonds (M = Ge, Ga, Sb) presumably present in such glass system specially for Se-deficit glasses but also in order to compensate the presence of Se in short chains between two units among [Ge(Ga)$Se_{4/2}$] and [$SbSe_{3/2}$] entities [20, 27] which is the case in studied selenide glass with the presence of Ge-Ge bonds leading to a contribution at 170 cm^{-1}. Considering the Ge–Ge bonds vibration modes in [Ge–Ge_mSe_{4-m}] - including Se_3Ge-$GeSe_3$ ethane like - structural units, already observed in amorphous Ge-rich composition, a small wide band centered at ~270 cm^{-1} can be expected. Finally, the small Raman band spreading from 285 to 310 cm^{-1} can be related to the asymmetric stretching modes of Td-CS (305 cm^{-1}), more clearly observed in IR spectrum as previously mentioned, with a contribution due to the presence of [$GaSe_{4/2}$] tetrahedra. In this spectral region, theoretical vibrational modes calculated by DFT are present at 300 cm^{-1} for asymmetric stretching mode of [$GeSe_{4/2}$] Td-CS mostly active in IR [21–23], but also at 310 and 288 cm^{-1} for active Raman mode of Td-ES and Se_3Ge-$GeSe_3$ethanelike entities, respectively proposed in [21] or at 311 cm^{-1} and 285 cm^{-1} for asymmetric stretching mode of Td-ES more active in IR spectrum [22].

The introduction of tellurium instead of selenium with a [Te/(Se + Te)] ratio of between 15.4% and 57.7% progressively affects the IR spectra while a drastic change of the Raman spectra is visible. The latter are shifted very significantly towards lower wavenumbers with a sharp decrease in the intensity of dominant band peaking at 190-215 cm^{-1} and the disappearance of the band at 265 cm^{-1} in favor of a wide band that first appears at 170 cm^{-1}

Optical Materials EXPRESS

and slips gradually to stabilize at 150 cm^{-1} for $Ga_5Ge_{20}Sb_{10}Se_{65-x}Te_x$ bulk glass with x ranging from 10 to 37.5%. These changes can be interpreted as follows. The contribution of [Ge(Ga)Se_4], [$SbSe_3$] and Se-Se entities seem to disappear quickly in favor of a wide band which is first centered at 170 cm^{-1} and then moves towards 150 cm^{-1}. We can reasonably assume that the incorporation of tellurium will lead to the formation of mixed entities such as [Ge(Ga)$Se_{4-x}Te_x$], [$SbSe_{3-x}Te_x$] and Se-$Se_{(n-x)}$-Te_x or Te-Te chains. The symmetrical stretching mode at 130 cm^{-1} associated with A_1 symmetric stretching mode of [$GeTe_{4/2}$] tetrahedra (Td) does not appear clearly in Raman spectra but the asymmetry of the band centered at 150 cm^{-1} can suggest a possible contribution of these entities [28–30]. The presence of mixed chains $Se_{(n-x)}$-Te_x between Ge, Sb, Ga based entities is expected around 200-220 cm^{-1} [31]; nevertheless, it cannot be clearly confirmed because this region also corresponds to the vibrational modes of [Ge(Ga)$Se_{4/2}$] entities which could still remain present within the structure of the glasses. Due to the stoichiometry of fabricated glasses, it seems very reasonable to associate the main Raman band with vibrational modes of the mixed entities [Ge(Ga)$Se_{4-x}Te_x$] and [$SbSe_{3-x}Te_x$]. This is in agreement with the DFT calculations of R. Mereau who proposes a symmetric stretching vibration mode for a mixed tetrahedron [$GeSe_{2/2}Te_{2/2}$] at 170 cm^{-1} [22]. By comparing the latter to the mode of the [$GeTe_{4/2}$] Td at 130 cm^{-1}, we can expect a shift of this mode of vibration from 170 cm^{-1} to 130 cm^{-1} with increasing substitution of Se by Te in the mixed tetrahedra. It was also proposed that a Raman active band around 145 cm^{-1} originates from Sb-Te vibrations in [$SbTe_{3/2}$] pyramidal units or defective octahedral [32–34].

Despite of the fact that substantial differences between IR spectra of studied glasses are not observed with increasing Te content, there are nevertheless variations of the distribution of the vibrational modes with several bands appearing and disappearing. The band at 155 cm^{-1} appearing from x = 20% of Te is accompanied by the progressive decay of the band at 200 cm^{-1}. Furthermore, the very gradual displacement of the band at 262 cm^{-1} towards 250 $cm^{-1}$is complemented by the regular vanishing of the 305 cm^{-1} band moving to 283 cm^{-1}. Finally, from x = 30% of Te, we can clearly see a shoulder at 220 cm^{-1}. The formation of mixed Se-Te entities such as [Ge(Ga)$Se_{4-x}Te_x$] is at the origin of the shift of the main asymmetric stretching modes of [Ge(Ga)Se_4] Td, initially centered at 262 and 305 cm^{-1}, to 250 and 283 cm^{-1}, respectively. We suppose that the appearance of the IR band at 150 cm^{-1} could be associated with the vibrational modes of Sb-Te bonds in the [$SbTe_{3/2}$] entities at the expense of the [$SbSe_{3/2}$] ones causing the gradual intensity decrease of the IR band at 200 cm^{-1}.

An important point of the vibrational data analysis concerns the non-radiative relaxations of excited Tb^{3+} ions via interactions with the phonons of the vitreous matrix. Although the main vibration modes active in Raman spectra become the ones around 150 cm^{-1} for a [Te/Se] ratio between 45 and 58%, it is also important to consider the modes active in IR spectroscopy. They are localized around 250-300 cm^{-1}, which is a phonon energy range remaining relatively high to clearly favor mid-IR luminescence in the 8-9 µm region compare to pure selenium matrix. The Fig. 4 shows the refractive indices dispersion curves determined by the VASE data analysis with Sellmeier model. As the polarizability of the chalcogenide elements increases with the weight and electronic density, the substitution of Te instead of Se induces an increase of the refractive index for the chalcogenide glasses from 2.56 to 2.55 for x = 0 to 3.11-3.07 for x = 35 within λ = 2.1-4.8 µm range.

Optical Materials EXPRESS

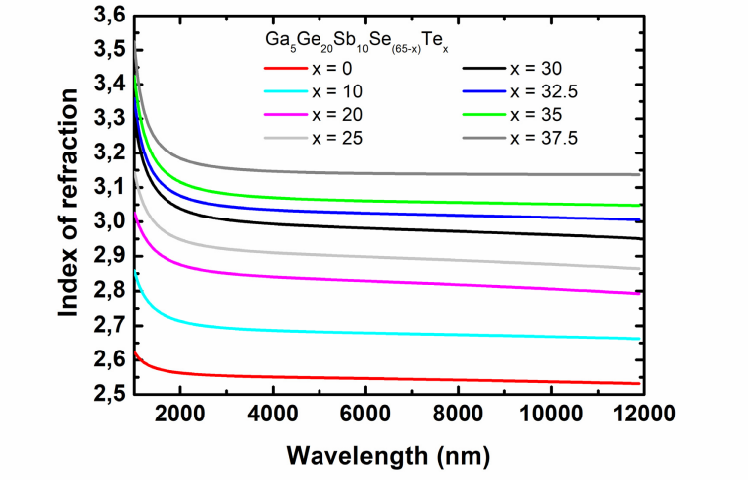

Fig. 4. Refractive index dispersion of bulk $Ga_5Ge_{20}Sb_{10}Se_{65-x}Te_x$ glasses.

Based on above described analysis of the $Ga_5Ge_{20}Sb_{10}Se_{65-x}Te_x$ glasses properties, we decided to select two compositions for photoluminescence study in MWIR and LWIR:(i) $Ga_5Ge_{20}Sb_{10}Se_{65}$considering that it is a composition already known, which can serve as a reference for drawing efficient fiber active in IR [35] and (ii) $Ga_5Ge_{20}Sb_{10}Se_{45}Te_{20}$ in order to have a material with wide transparency in near- and mid-IR offering lower phonon energy. This composition has been also selected regarding the ΔT parameter which is suitable for fiber drawing. Finally, the proportion of [Te/(Te + Se)] about 30% is still large enough to affect spectroscopic properties of incorporated Tb^{3+} ions.

3.2. Fiber attenuation

The fiber optical attenuation curves given in Fig. 5 show a minimum optical loss of about 1.3 and 4 dB/m for 500 ppm Tb^{3+} doped $Ga_5Ge_{20}Sb_{10}Se_{65}$ and $Ga_5Ge_{20}Sb_{10}Se_{45}Te_{20}$ fibers, respectively. The higher optical attenuation recorded for the seleno-telluride fiber could be explained by larger intrinsic losses coming from the presence of free charge carriers which degrade the optical properties [36].

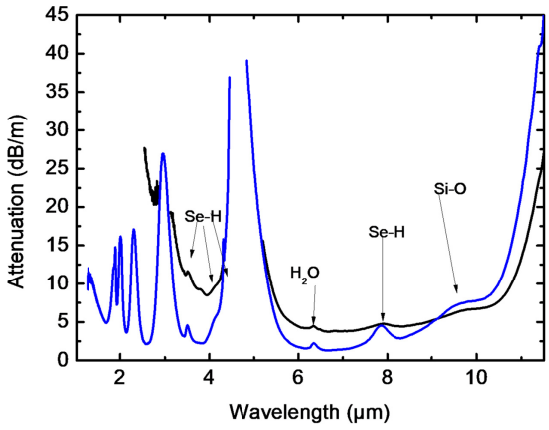

Fig. 5. Attenuation curves of 500 ppm Tb^{3+} doped $Ga_5Ge_{20}Sb_{10}Se_{65}$ (blue curve) and $Ga_5Ge_{20}Sb_{10}Se_{45}Te_{20}$ fibers (black curve).

Optical Materials EXPRESS

Comparing the two attenuation curves, the selenide fiber present logically an electronic and a multi-phonon cut-off at lower wavelengths compare to those of the seleno-telluride fiber. The [Se-H] absorption band at 7.9 µm is more important in selenide fiber which is a consequence of higher content of [Se-H] impurity in selenide fiber (~33 ppm) in contrast with seleno-telluride fiber (~20 ppm) considering the undoped fiber.

3.3. Tb^{3+} ions spectroscopic properties

Spectral dependencies of absorption coefficients were recorded for both 500 ppm Tb^{3+} doped $Ga_5Ge_{20}Sb_{10}Se_{45}Te_{20}$ and $Ga_5Ge_{20}Sb_{10}Se_{65}$ bulk glasses. Data presented in Fig. 6(a) indicate absorption bands attributed to the $^7F_6 \rightarrow {}^7F_{5,4,3,2,1}$ transitions. The corresponding simplified energy diagram is reported in Fig. 6(b). This indicates good rare earth incorporation in both glasses thanks to the presence of Ga atoms. Note that the $^7F_6 \rightarrow {}^7F_4$ and $^7F_6 \rightarrow {}^7F_5$ absorption bands are overlapped with the [O-H] and [Se-H] impurity absorption bands, respectively. An overlap between two absorption peaks for $Ga_5Ge_{20}Sb_{10}Se_{45}Te_{20}$ glass is observed. The shoulder at higher wavelength than [Se-H] entities could be attributed to [Ge-H] impurity absorption bands, expected at 4.9 µm, [As-H] impurity as also an absorption band around 5 µm thus an absorption band related to [Sb-H] could be also present at 5.1-5.2 µm, finally [Te-H] could be also expected in this spectral range. This is why for the J-O calculations, to estimate the true absorption cross-section of the $^7F_6 \rightarrow {}^7F_5$ and $^7F_6 \rightarrow {}^7F_4$ transitions, the absorption coefficient spectra were corrected for impurities absorption contributing to the overall absorption. For the corrections, absorption measurements of undoped glasses were exploited.

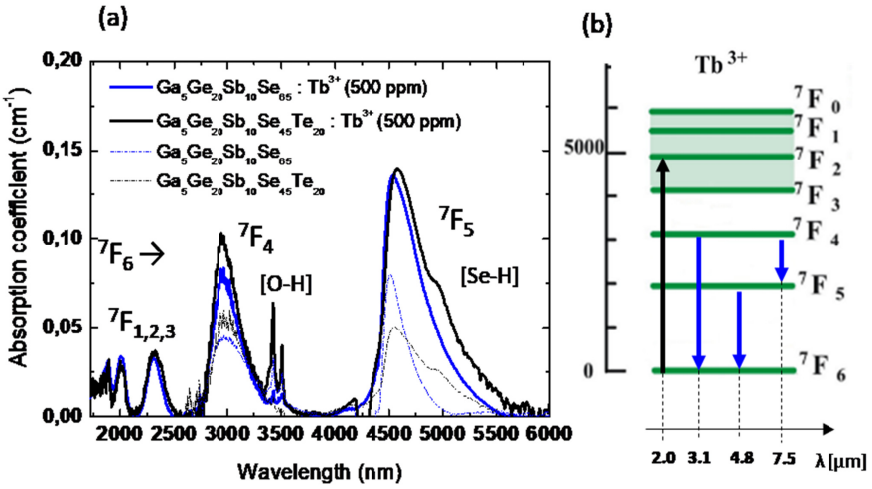

Fig. 6. (a) Absorption coefficient of 500 ppm Tb^{3+} doped $Ga_5Ge_{20}Sb_{10}Se_{65}$ and$Ga_5Ge_{20}Sb_{10}Se_{45}Te_{20}$ bulk glass and (b) the simplified energy level diagram of Tb^{3+} ion with expected MWIR and LWIR luminescence transitions.

The J-O parameters were calculated from the absorption cross-sections following a standard fitting procedure and magnetic dipole contributions calculations [37]. The main results of J-O calculations are reported in Table 2. The calculated $\Omega_{2,4,6}$ parameters are (4.9, 4.6, 1.6).10^{-20} cm^2 and (6.1, 3.2, 0.9).10^{-20} cm^2 for Tb^{3+}:$Ga_5Ge_{20}Sb_{10}Se_{65}$ and Tb^{3+}:$Ga_5Ge_{20}Sb_{10}Se_{45}Te_{20}$, respectively. Interestingly, when the impurities absorption bands are not subtracted from the Tb^{3+} transitions related absorption bands, it would lead to a 20% relative error for the calculated radiative lifetimes. For example, τ_{rad} of $^7F_5$ level was estimated as 13.9 and 11.4 ms with and without impurities correction for Tb^{3+}:$Ga_5Ge_{20}Sb_{10}Se_{65}$ glass, respectively. Note that the Ω_2 parameter values are driven by the

Optical Materials EXPRESS

unique $^7F_6 \rightarrow {}^7F_5$ absorption transition, as the $(U_2)^2$ matrix element is one order of magnitude larger for this transition. Moreover, this $(U_2)^2$ element is equal to zero for the $^7F_6 \rightarrow {}^7F_3$ and $^7F_2$ related absorption bands. To conclude, major discrepancies in the J-O calculations may occur when the appropriate subtraction of the impurities contribution to the adjacent Tb^{3+} absorption band ($^7F_6 \rightarrow {}^7F_5$ transition) is not performed.

Table 2. Calculated radiative properties of infrared transitions in 500 ppm Tb^{3+} doped $Ga_5Ge_{20}Sb_{10}Se_{65}$/$Ga_5Ge_{20}Sb_{10}Se_{45}Te_{20}$ glasses for observed emissions centered at wavelength λ, with quantum efficiency η. $A^{ED}$and A^{MD} stand for spontaneous electronic and magnetic emission rates, respectively. β_{rad} are corresponding branching ratios. τ_{rad} and τ_{exp} represent radiative and experimental lifetimes, respectively.

Tb^{3+}:$Ga_5Ge_{20}Sb_{10}Se_{65}$							
Transition	λ (μm)	A^{ED}[s^{-1}]	A^{MD}[s^{-1}]	β	τ_{rad}[ms]	τ_{exp}[ms]	η
$^7F_5 \rightarrow {}^7F_6$	4.8	64.9	6.9	1	13.9	8.9	0.64
$^7F_4 \rightarrow {}^7F_5$	7.9	10.3	2.7	0.07	4.9	-	-
$^7F_4 \rightarrow {}^7F_6$	3.1	187	0	0.93			
Tb^{3+}:$Ga_5Ge_{20}Sb_{10}Se_{45}Te_{20}$							
Transition	λ (μm)	A^{ED}[s^{-1}]	A^{MD}[s^{-1}]	β	τ_{rad}[ms]	τ_{exp}[ms]	η
$^7F_5 \rightarrow {}^7F_6$	4.8	60.4	6.9	1	14.8	7.8	0.52
$^7F_4 \rightarrow {}^7F_5$	7.9	11.1	2.7	0.09	6.5	-	-
$^7F_4 \rightarrow {}^7F_6$	3.1	140	0	0.91			

Performed J-O calculations show that magnetic and electric dipole strengths of Tb^{3+} transitions are very close to those reported for a selenide material where antimony is substituted by arsenic [14]. The $\Omega_{2,4,6}$ parameters obtained in this work are also comparable, resulting in similar values of calculated radiative lifetimes. The calculated $^7F_5$ decay lifetime (13.9 ms) obtained for the pure selenide glass sample is in good agreement with the value calculated for a Ga-Ge-As-Se glass sample (13.1 ms) [14]. In the present work, longer Tb^{3+} ions radiative lifetimes are found for seleno-telluride than for selenide glasses ($^7F_5$ level lifetime ~14.8 and ~13.9 ms for $Ga_5Ge_{20}Sb_{10}Se_{45}Te_{20}$ and $Ga_5Ge_{20}Sb_{10}Se_{65}$ matrix, respectively). On the other hand, the measured fluorescence lifetimes of the $^7F_5$ manifold are equal to 7.8 and 8.9 ms for $Ga_5Ge_{20}Sb_{10}Se_{45}Te_{20}$ and $Ga_5Ge_{20}Sb_{10}Se_{65}$ glass, respectively. Both $^7F_5$ manifold fluorescence lifetimes are in good agreement with the experimental fluorescence lifetimes reported in the literature [13]. Presented values enable an estimation of the manifold quantum efficiency η in these materials ($\eta = \tau_{exp}/\tau_{rad}$). The η is found to be lower for Te containing glasses (~52%) compare to selenide glass (~64%), which seems to be a drawback for efficient infrared luminescence when adding Te in the selenide matrix.

Either on bulk or fiber samples, the emitted fluorescence in any studied spectral domain exhibits a higher magnitude for samples without Te. The quenching of the Tb^{3+} luminescence is somewhat stronger in $Ga_5Ge_{20}Sb_{10}Se_{45}Te_{20}$ than in $Ga_5Ge_{20}Sb_{10}Se_{65}$ glass composition likely related to dipole-dipole due to clustering of Tb^{3+} ions or electron-dipole interactions with mainly impurities like [OH] or [SeH]. For the same incident power, the MWIR luminescence is brighter with a Tb^{3+}:$Ga_5Ge_{20}Sb_{10}Se_{65}$ fiber, and exhibits a larger signal-to-noise ratio (Fig. 7(a), 7(b)) indicating a greater radiation quenching in the Tb^{3+}: $Ga_5Ge_{20}Sb_{10}Se_{45}Te_{20}$ material.

Optical Materials EXPRESS

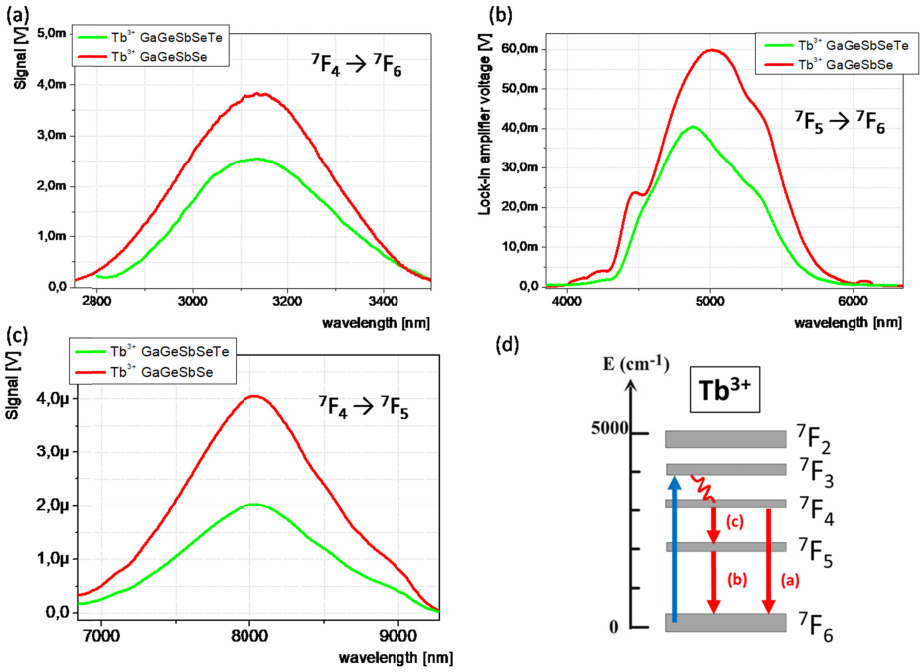

Fig. 7. Emission spectra of 500 ppm Tb^{3+} doped $Ga_5Ge_{20}Sb_{10}Se_{65}$ and $Ga_5Ge_{20}Sb_{10}Se_{45}Te_{20}$ fibers under excitation at λ = 2.05µm: (a) $^7F_4 \rightarrow {}^7F_6$ (3.1 µm) transition; (b) $^7F_5 \rightarrow {}^7F_6$ (4.7 µm) transition; (c) $^7F_4 \rightarrow {}^7F_5$ (8.0 µm); (d) Tb^{3+} low-lying manifolds energy diagram corresponding to the measured (a), (b) and (c) spectrums.

The reabsorption associated with the presence of [Se-H] entities is clearly observed at ~4.5 µm in the luminescence spectrum of the selenide fiber. This reabsorption phenomenon is less intense in the case of the seleno-telluride fiber probably because of a lower proportion of selenium in the vitreous network (Fig. 7(b)). Consequently, reabsorption results in a luminescence peak shift from 4.8 to 5.0 µm in the case of the selenide-based glasses. A key result is the observation of the $^7F_4$ emission at 3.1 µm for both selenide and seleno-telluride glasses. As depicted in Fig. 7(a), the $^7F_4 \rightarrow {}^7F_6$ emission at 3.1 µm with a good signal-to-noise ratio was recorded, evidencing rather strong emission from the $^7F_4$ manifold. Obviously non-radiative and radiative relaxation processes compete, but thanks to the low phonon energy of the chalcogenide matrix, the multiphonon relaxation process does not fully impair the $^7F_4 \rightarrow {}^7F_6$ radiative transition. This is a stimulating clue that an emission at 8.0 µm originating in $^7F_4 \rightarrow {}^7F_5$ transition could potentially exist in these materials. In fact, a well-defined ~8 µm luminescence from pure selenide glasses was demonstrated in Tb^{3+}:$Ga_5Ge_{20}Sb_{10}Se_{65}$ [12], and this result is compared in this article with the Tb^{3+} doped seleno-telluride glass.

The LWIR emission spectra of these two materials are reported in Fig. 7(c). Following the same trend as the 3.1 µm luminescence spectra, the ~8.0 µm emitted intensity is lower in the case of the Te-containing fiber compare to pure selenide fiber. The expectations coming from the substitution of Te instead of Se in the selenide glass matrix cover typically a decrease of the phonon energy (observed in Raman spectra in Fig. 3), increase of the refractive index (Fig. 4) and also red-shift of the cut-off wavelength in the transmission spectra (Fig. 2). However, the dispersion of rare earths seems to be less efficient in seleno-telluride materials. Moreover, the presence of impurities is comparable despite the purification processes. Finally, when looking at the vibration modes by both Raman and IR techniques, phonon energy of seleno-telluride glasses is almost as high as that of pure selenides glasses. Above described considerations lead to shorter lifetimes measured for the Te-containing glasses.

Optical Materials EXPRESS

Nevertheless, the radiative emissions observed especially at ~8.0 µm remain remarkable for seleno-telluride glasses. To obtain optimal luminescent properties for the highly sought luminescence at 8 µm, the next challenge is to decrease the impurity contain of such glasses by purification steps. Thus replacing Se by Te in the chalcogenide glass matrix remains a promising route to obtain better quantum efficiency of LWIR radiative transitions of rare earth ions incorporated in chalcogenide glasses.

4. Conclusions

Bulk $Ga_5Ge_{20}Sb_{10}Se_{65-x}Te_x$ with x = 0, 10, 20, 25, 30, 32.5, 35, 37.5 chalcogenide glasses and 500 ppm Tb^{3+} doped $Ga_5Ge_{20}Sb_{10}Se_{65}$ or $Ga_5Ge_{20}Sb_{10}Se_{45}Te_{20}$ chalcogenide glasses/fibers were synthesized with a deep control of their purity. Tb^{3+} ions are efficiently introduced into $Ga_5Ge_{20}Sb_{10}Se_{65}$ or $Ga_5Ge_{20}Sb_{10}Se_{45}Te_{20}$ glasses. We observe MWIR emission in the range of 4.3-6.0 µm attributed to the $^7F_5 \rightarrow {}^7F_6$ transition with a corresponding experimental lifetime of 8.9 and 7.8 ms for the selenide and seleno-telluride matrix, respectively. An emission from the $^7F_4$ level is measured in the spectral range of 2.8-3.4 µm which is a first step towards the challenge to observe the 8.0 µm luminescence from studied Tb^{3+}:$Ga_5Ge_{20}Sb_{10}Se_{65-x}Te_x$ materials. This LWIR emission was also measured for the Tb^{3+}:$Ga_5Ge_{20}Sb_{10}Se_{45}Te_{20}$ fiber. Although a lower intensity than that of the selenide matrix has been observed, it still remains very appreciable. The unambiguous observation of the 8.0 µm emission band in Tb^{3+}: $Ga_5Ge_{20}Sb_{10}Se_{65-x}Te_x$ (x = 0 and 20) opens up new prospects for the mid-IR sensors, especially in the field of the gas remote sensors.

Funding

Optigas ANR project (ANR-15-CE39-0007); Czech Science Foundation (Project No. 16-17921S).